Contract No. and Disclaimer:

This manuscript has been authored by Savannah River Nuclear Solutions, LLC under Contract No. DE-AC09-08SR22470 with the U.S. Department of Energy. The United States Government retains and the publisher, by accepting this article for publication, acknowledges that the United States Government retains a non-exclusive, paid-up, irrevocable, worldwide license to publish or reproduce the published form of this work, or allow others to do so, for United States Government purposes.

Reversible Hydrogen Storage in a $LiBH_4$-C_{60} Nanocomposite

Patrick A. Ward,[†] *Joseph A. Teprovich Jr.,*[‡] *Brent Peters,*[‡] *Joseph Wheeler,*[‡] *Robert N. Compton,*[†] *Ragaiy Zidan*[‡*]

[†]Department of Chemistry, University of Tennessee, Knoxville, TN 37996, USA

[‡]Clean Energy Directorate- Savannah River National Laboratory, Aiken, SC 29801, USA

*email: ragaiy.zidan@srnl.doe.gov

Hydrogen storage, fullerene, $LiBH_4$, nanocomposite, fullerane

Reversible hydrogen storage in a $LiBH_4$:C_{60} nanocomposite (70:30 wt. %) synthesized by solvent-assisted mixing has been demonstrated. During the solvent-assisted mixing and nanocomposite formation, a chemical reaction occurs in which the C_{60} cages are significantly modified by polymerization as well as by hydrogenation (fullerane formation) in the presence of $LiBH_4$. We have determined that two distinct hydrogen desorption events are observed upon rehydrogenation of the material, which are attributed to the reversible formation of a fullerane ($C_{60}H_x$) as well as a $LiBH_4$ species. This system is unique in that the carbon species (C_{60}) actively participates in the hydrogen storage process which differs from the common practice of

melt infiltration of high surface area carbon materials with $LiBH_4$ (nanoconfinment effect). This nanocomposite demonstrated good reversible hydrogen storage properties as well as the ability to absorb hydrogen under mild conditions (pressures as low as 10 bar H_2 or temperatures as low as 150°C). The nanocomposite was characterized by TGA-RGA, DSC, XRD, LDI-TOF-MS, FT-IR, ^{1}H NMR, and APPI MS.

1. Introduction

Lithium borohydride ($LiBH_4$) is of great interest for hydrogen storage due to its high gravimetric capacity of 18.4 wt. % if complete desorption is achieved (13.8 wt. % for $LiBH_4 \rightarrow LiH + B + 3/2\ H_2$). However, its use in hydrogen storage applications is problematic due to poor hydrogen desorption/absorption kinetics, the release of volatile gases (B_2H_6), and formation of stable byproducts ($Li_2B_{12}H_{12}$).[1, 2] Diborane emission and $Li_2B_{12}H_{12}$ production limit the amount of accessible hydrogen uptake in the material over multiple cycles. Like many other complex hydrides, there have been numerous reports demonstrating improvement of the hydrogenation/dehydrogenation kinetics of $LiBH_4$ through the combination of high energy milling with other metal hydrides and/or incorporation of transition metal salts.[3]

More recently it has been demonstrated that melt infiltration of $LiBH_4$ into porous materials is a promising alternative to high energy milling and transition metal doping. The incorporation of $LiBH_4$ into carbon materials has been shown to lower the desorption temperature, improve the reversible formation of $LiBH_4$, and limit the amount of volatile byproducts. Improvements in the cycling of $LiBH_4$, in these systems, have been attributed to the "nano-confinment" effect. This effect is achieved by melting $LiBH_4$ (using elevated temperature and/or pressure) which can then infiltrate and fill the porous voids in the carbon scaffold effectively reducing the particle size of $LiBH_4$ leading to an enhancement of its hydrogen storage properties. It has been shown that

$LiBH_4$ can be incorporated into SBA-15, carbon aerogels, disordered mesoporous carbon (CMK-3), activated carbon, and CNT's which demonstrate the effect of nano-confinement.[2-15] One drawback to nanoconfinement-based systems is that the porous material acts as "dead weight" and there have been no reports of the porous material actively participating in the hydrogen storage process. The enhancements in hydrogen storage properties are attributed to a reduction of $LiBH_4$ particle size upon melt infiltration. In many cases, the weight percent of $LiBH_4$ nanoconfined in the porous matrix is typically between 20-70 wt. %, reducing the overall gravimetric hydrogen capacity of the composite material.

While it is plausible that the presence of C_{60} in our material may reduce the average particle size of $LiBH_4$, the evidence of two distinct desorption steps and the appearance of hydrogenated fullerenes (fulleranes) give compelling evidence for active participation of the fullerene in the absorption/desorption process. Recent theoretical work has suggested that C_{60} is an effective catalyst for reducing the desorption temperature of $LiBH_4$.[16] This effect is attributed to a sizeable reduction in the energy required to remove the first hydrogen atom from $LiBH_4$. The energy reduction is a consequence of increased stabilization of the product state. This is achieved through the formation of a 'substitution' bond between the B atom of $LiBH_3$ and a C atom of C_{60}. This newly formed bond is facilitated by a charge transfer reaction that is analogous to a previously proposed mechanism for the interaction of $NaAlH_4$ with C_{60}.[17] This similar mechanism, now involving two C atoms, is responsible for the even further reduced hydrogen removal energy when going from $LiBH_3$ to $LiBH_2$.

In our continuing efforts to understand the effect of C_{60} on the hydrogen storage properties of metal hydrides ($NaAlH_4$, $LiAlH_4$, etc.)[17-25], we have prepared a $LiBH_4$:C_{60} nanocomposite via solvent-assisted mixing and demonstrated reversible hydrogen storage with partial capacity

retention after 10 desorption cycles. We have determined that C_{60} lowers the desorption temperature of $LiBH_4$ as well as actively participating in the hydrogen storage process through the reversible formation of C-H bonds and $LiBH_4$.

2. Experimental

2.1 Materials

Chemicals were used as provided by the supplier and are listed by supplier as follows. Sigma-Aldrich: LiBH4, C_{60}, and THF (anhydrous, inhibitor-free).

2.2 Sample Preparation/Characterization

All manipulations of the samples were performed in an argon-filled glovebox or utilizing Schlenk line techniques. Samples were prepared by dissolving $LiBH_4$ and C_{60} (~1.0 g total) in 40 mL of THF with stirring for 5-12 hours. Solvent was then removed under vacuum and heat. The material was then lightly ground with a mortar and pestle followed by additional vacuum and heat to remove residual THF. This material is referred to as the "as prepared" sample. Dehydrogenation was performed by heating the sample to 530°C at 5°C/min followed by a 30 minute soak at 530°C under flowing argon on a Schlenk line. Rehydrogenation of the sample was performed on a HyEnergy PCT Pro 2000 instrument. The sample (200mg -750 mg) was first charged with hydrogen over pressure (10-100 bar H_2) then heated to the desired temperature (150-340°C) over 90 minutes, followed by isothermal conditions for 5 hours at the designated temperature.

A Perkin Elmer Thermogravimetric Analyzer-Pyris 1 TGA was used for TGA/RGA experiments. The sample was heated from 30 to 530˚C at a heating rate of 5˚C/min followed by isothermal conditions at 530 ˚C for 30 minutes, with a sample size of ~5mg. The weight percent lost during the heating is reported with respect to the total weight of the composite and not the

$LiBH_4$ content as described in many other reports. The gas released during the heating process was identified using a Hiden Analytical RGA. X-ray powder diffraction (XRD) was performed using a PANalytical X'pert Pro with Cu-Kα radiation, and the samples were protected with a Kapton® film to minimize oxidation of the sample. NMR spectra were recorded on a solution state Varian 500 MHz NMR with a relaxation time of 1.0 second and 256 scans. Samples were prepared under Ar in d_6-DMSO and sealed in air-tight NMR tubes. FT-IR measurements were carried out on a Thermo Scientific Nicolet IR100 FT-IR in a nitrogen filled glovebox. Samples were prepared as KBr pellets. Differential Scanning Calorimetry was performed on a Seteram SENSYS evo DSC using a heating rate of 5°C/min with a constant flow of Ar. The sample crucibles were sealed under Ar in a glovebox. Laser desorption time-of-flight mass spectra (LDI TOF MS) were measured on an AppliedBiosystems Voyager-DE Pro. Positive ion spectra were recorded using delayed pulse extraction in reflectron mode. Typical mass spectra resolution ($m/\Delta m$) was 2,500 calculated from the full-width half maximum. Samples were prepared by dissolving 1 mg of sample in 1 mL of anhydrous benzene or THF then spotting 1uL of the solution on the sample plate under an Ar atmosphere.

3. Results and Discussion

We prepared a $LiBH_4$:C_{60} (77:1 mol ratio, 70:30 weight ratio) nanocomposite via a solvent-assisted mixing method to make an "as prepared" (heat and vacuum dried) sample which was then dehydrogenated and rehydrogenated under various conditions. These samples were then subjected to a series of spectroscopic and thermo-analytical techniques in order to understand the mechanism of hydrogen release and absorption, as well as the composition of the material at each stage of cycling. An advantage of the solvent-assisted mixing process is the ability to easily prepare large quantities of material without the introduction of fullerene cage

defects or metal contaminants, which are associated with commonly used high-energy milling techniques.

3.1 Hydrogen Desorption/Absorption

Figure 1 shows the TGA-RGA comparisons of the first desorption of $LiBH_4$- C_{60} (from the as prepared sample) versus pure $LiBH_4$. This first desorption clearly shows that the temperature of the primary desorption event is significantly lowered relative to pure $LiBH_4$ in the presence of C_{60} than without. Upon heating to 530°C, a weight loss of 13.0 wt. % from the $LiBH_4$:C_{60} nanocomposite is observed which is very close to the theoretical hydrogen capacity of ~12.9 wt. % H_2 for this material. This additional weight loss is attributed to residual THF in the sample, which is the small weight loss event occurring before the onset of H_2 desorption (~275°C).

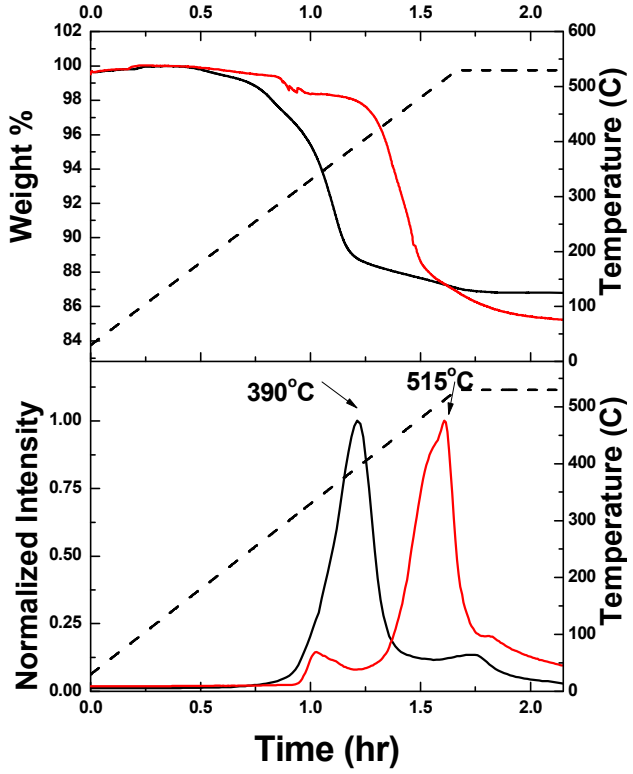

Figure 1. TGA (top) and RGA (Bottom) of pure LiBH4 (red) and LiBH4:C60 as prepared (black) with temperature (dashed line). Heating rate was 5°C/minute (30°C to 530°C) followed by 30 minutes at 530°C.

The RGA shows that there are two distinct desorption events occurring during the dehydrogenation of the $LiBH_4$:C_{60} composite. The first desorption event is dominant with the second desorption event a minor component occurring at a higher temperature than the main desorption of pure $LiBH_4$. Also, the maximum rate of desorption for the $LiBH_4$:C_{60} material occurs 125°C lower than the pure $LiBH_4$ sample.

Utilizing the Kissinger method[26] the activation energy (E_a) for the desorption of $LiBH_4$ in the $LiBH_4$:C_{60} composite was determined and compared to the E_a for bulk $LiBH_4$. For pure $LiBH_4$ an activation energy of 133 ±2 kJ/mol was measured, which is lower than the previously determined E_a values for bulk $LiBH_4$ of 156 ±20 kJ/mol[27] and 146 ±3 kJ/mol.[9] In the presence of $C_{60,}$ the activation energy of $LiBH_4$ is lowered to 108 ±11 kJ/mol for the first desorption from the as prepared material. After rehydrogenation, the 2nd desorption of the material yielded an activation energy of 113 ±7 kJ/mol, which is consistent with the 1st desorption from the as prepared $LiBH_4$:C_{60} material, within experimental error. This value is close to that reported for $LiBH_4$ in a carbon aerogel (111 ±2kJ/mol) with a pore size of 25nm utilizing the Ozawa analysis.[9] This indicates that C_{60} has a catalytic effect by lowering the energy barrier for the release of H_2 from $LiBH_4$.

The DSC profile of the same materials (~17 mg samples each) in the hydrogenated state is shown in Figure 3. There is a slight reduction (117°C from 118°C) in the temperature for the phase transition from orthorhombic to hexagonal in the $LiBH_4$:C_{60} versus bulk $LiBH_4$. Upon rehydrogenation of the sample, the DSC signal for this phase transition is significantly reduced

and shifted to lower temperature (104ºC) for the 2nd desorption. The melting temperature of LiBH4 is also slightly reduced during the first desorption from 290°C to 287°C in the "as prepared" material. The melting point of the $LiBH_4$:C_{60} composite is further reduced to 274°C for the second desorption of the material.

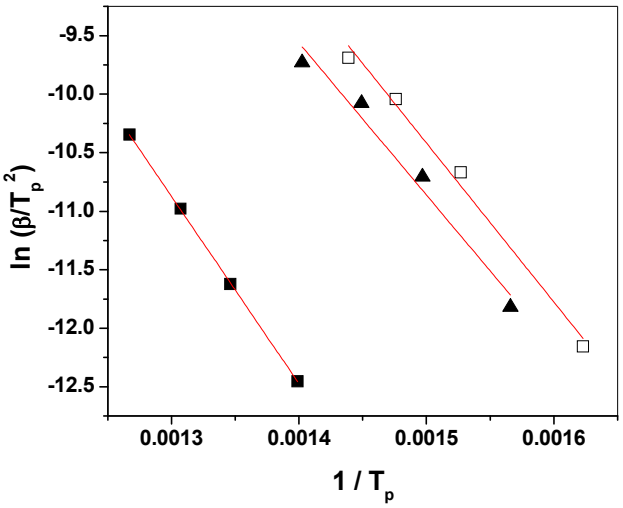

Figure 2. Kissinger Plot obtained by TGA data at different heating rates for pure $LiBH_4$ (■), $LiBH_4$:C_{60} as prepared (▲), and $LiBH_4$:C_{60} after first rehydrogenation (□).

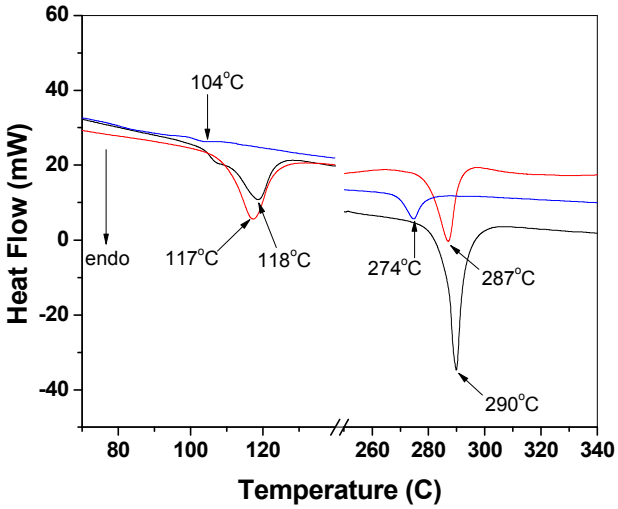

Figure 3. DSC curves for pure $LiBH_4$ (black), $LiBH_4$:C_{60} as prepared (red), and $LiBH_4$:C_{60} after first rehydrogenation (blue).

We also observed that the amount of "foaming" typically associated with the dehydrogenation of $LiBH_4$ is significantly reduced in the $LiBH_4$:C_{60} nanocomposite (Figure 4). In this experiment, both of the samples were heated to 530ºC under argon flow on a Schlenk line. The pure $LiBH_4$ (0.1g sample) showed a significant volume expansion during the dehydrogenation, while the $LiBH_4$:C_{60} (0.2g sample) showed a minimal amount of volume expansion in the dehydrogenated state even though twice the amount of sample was tested. The $LiBH_4$:C_{60} sample formed a solid chunk at the base of the vial. The minimal volume expansion and close contact of the $LiBH_4$:C_{60} decomposition products may ultimately lead to the improved reversible hydrogenation of the material at lower temperatures and pressures required for pure $LiBH_4$.

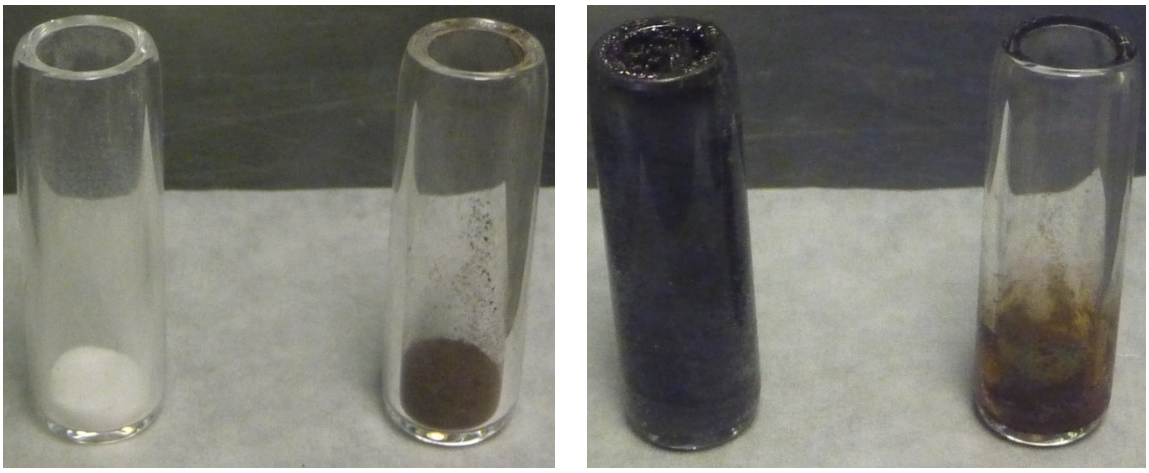

Figure 4. Photographs of $LiBH_4$ (0.1g, white) and $LiBH_4$:C_{60} (0.2g, brown) before (left pane) and after dehydrogenation (right pane).

3.2 Effect of Temperature and Pressure on Hydrogen Capacity

The $LiBH_4$:C_{60} composite was rehydrogenated at varying temperatures and pressures in order to determine the optimal conditions for hydrogen uptake by the material. TGA-RGA was utilized to determine the amount of hydrogen uptake in these samples. Figure 5 shows the effect of hydrogenation temperature on hydrogen uptake by the material. The TGA data illustrates a

higher degree of hydrogenation at higher temperatures. The normalized RGA data shows an increasing ratio of the lower temperature desorption step compared to the higher temperature desorption step, respectively. Since, the first desorption step is attributed to the dehydrogenation of $LiBH_4$, this indicates more $LiBH_4$ being regenerated at higher temperatures. The change in weight loss from the 2nd desorption step varies only slightly (increases with temperature) at different temperatures which is consistent with the dehydrogenation of fulleranes.

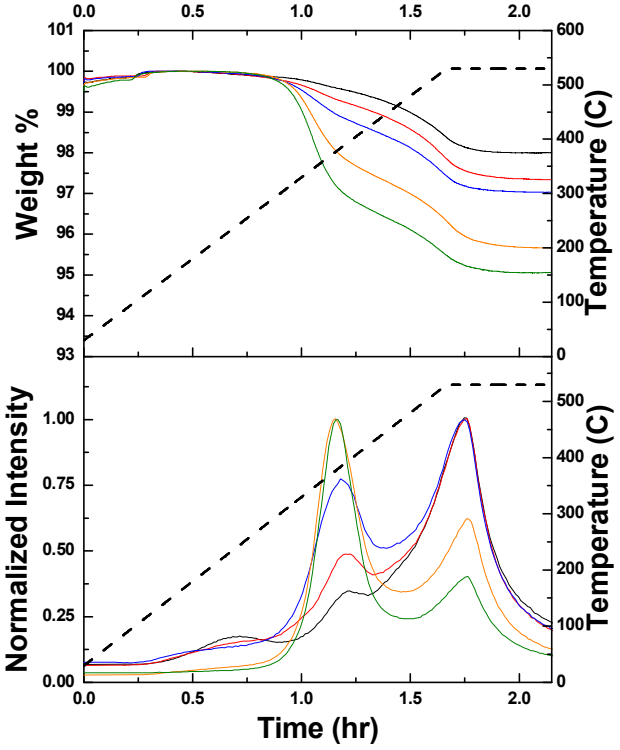

Figure 5. TGA/RGA of the rehydrogenated $LiBH_4$:C_{60} material (after 1st desorption of as prepared material) rehydrogenated at various temperatures at 100 bar H_2 pressure for 5 hours. Black- 150°C, red- 200°C, blue- 250°C, orange- 300°C, and green- 330°C.

As shown in Figure 6, increasing hydrogenation overpressure results in higher hydrogen uptake by the material. Similar to the temperature dependence, higher pressures result in more $LiBH_4$ regeneration. It is obvious that C_{60} plays a major role in the reversibility of $LiBH_4$

considering that pure $LiBH_4$ requires significantly higher temperatures (600 °C) and pressures (350 bar) for the regeneration of pure $LiBH_4$ after it's dehydrogenation.[28]

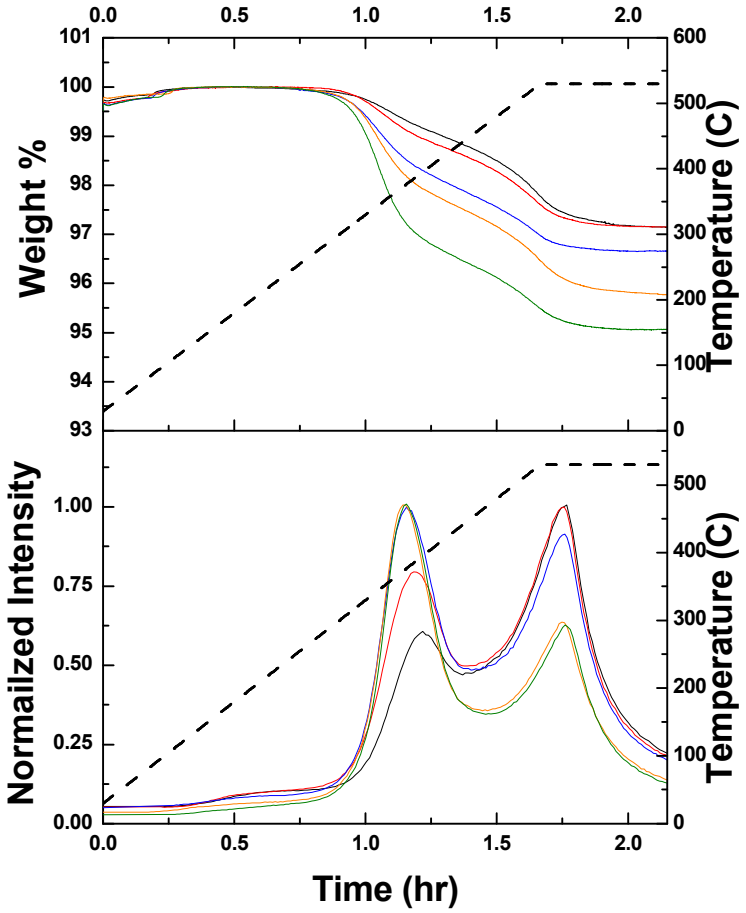

Figure 6. TGA/RGA of the rehydrogenated $LiBH_4$:C_{60} material (after 1st desorption of as prepared material) at various pressures at a constant temperature of 330 °C for 5 hours. Black- 10 bar H_2, red- 25 bar H_2, blue- 50 bar H_2, orange- 75 bar H_2, and green- 100 bar H_2.

3.3 Cycling

The $LiBH_4$:C_{60} material was rehydrogenated 8 times at 330 °C and a H_2 pressure of 100 bar to demonstrate the reversibility in the material over many cycles. TGA/RGA data for the cycles are shown below in Figure 7. The normalized RGA measurements show an increase in the

ratio of hydrogen release from fulleranes compared to $LiBH_4$, respectively, suggesting a decrease in $LiBH_4$ regeneration (as the cycle number increases). There is also a decrease in hydrogen capacity which stabilizes around ~3 wt. % (w.r.t. the entire composite) by the 6th cycle. This is explained by a decreased regeneration of $LiBH_4$ after cycling, which is likely caused by fullerene modification (polymerization or cage rupture), volatile B_2H_6 release, and formation of $Li_2B_{12}H_{12}$ or a combination of these decomposition mechanisms.

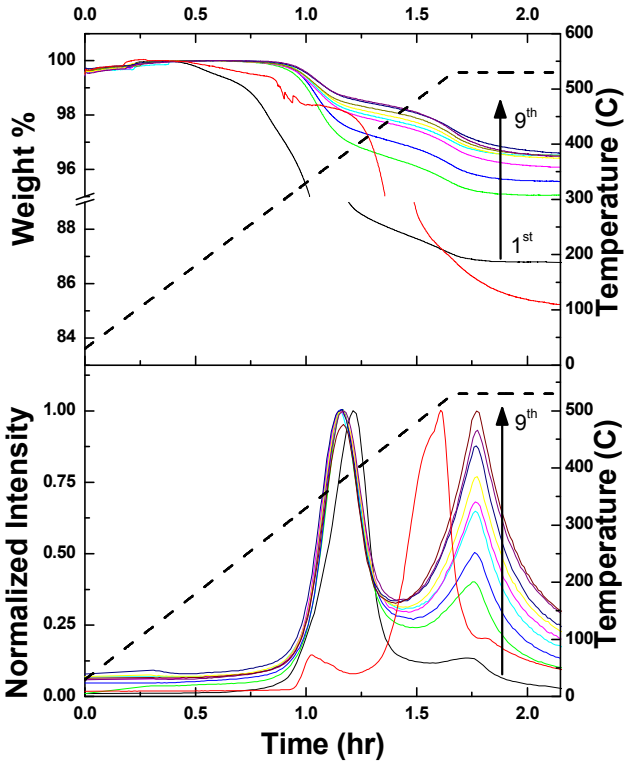

Figure 7. TGA/RGA analysis of the first 9 dehydrogenation cycles of the $LiBH_4$:C_{60} composite versus pure $LiBH_4$ (red). Rehydrogenation at 100 bar H_2, 330°C, for 5 hours.

3.4 APPI-MS

Atmospheric pressure photoionization mass spectra (APPI-MS) clearly show hydrogenated fullerenes in the "as prepared" material, figure 8, which is in agreement with LDI-TOF-MS measurements (Supporting Information). The "as-prepared" material was also synthesized without heating (to remove residual solvent) in order to determine if heating was responsible for the observation of fullerane ions in the mass spectra. Evidence of fulleranes in the material synthesized at room temperature demonstrates that C_{60} can be reduced at room temperature by $LiBH_4$. There is still evidence for trace amounts of $C_{60}H_{18}$ in the dehydrogenated sample, supporting the hypothesis that dehydrogenation of fulleranes is responsible for the second desorption step observed in the TGA/RGA data.

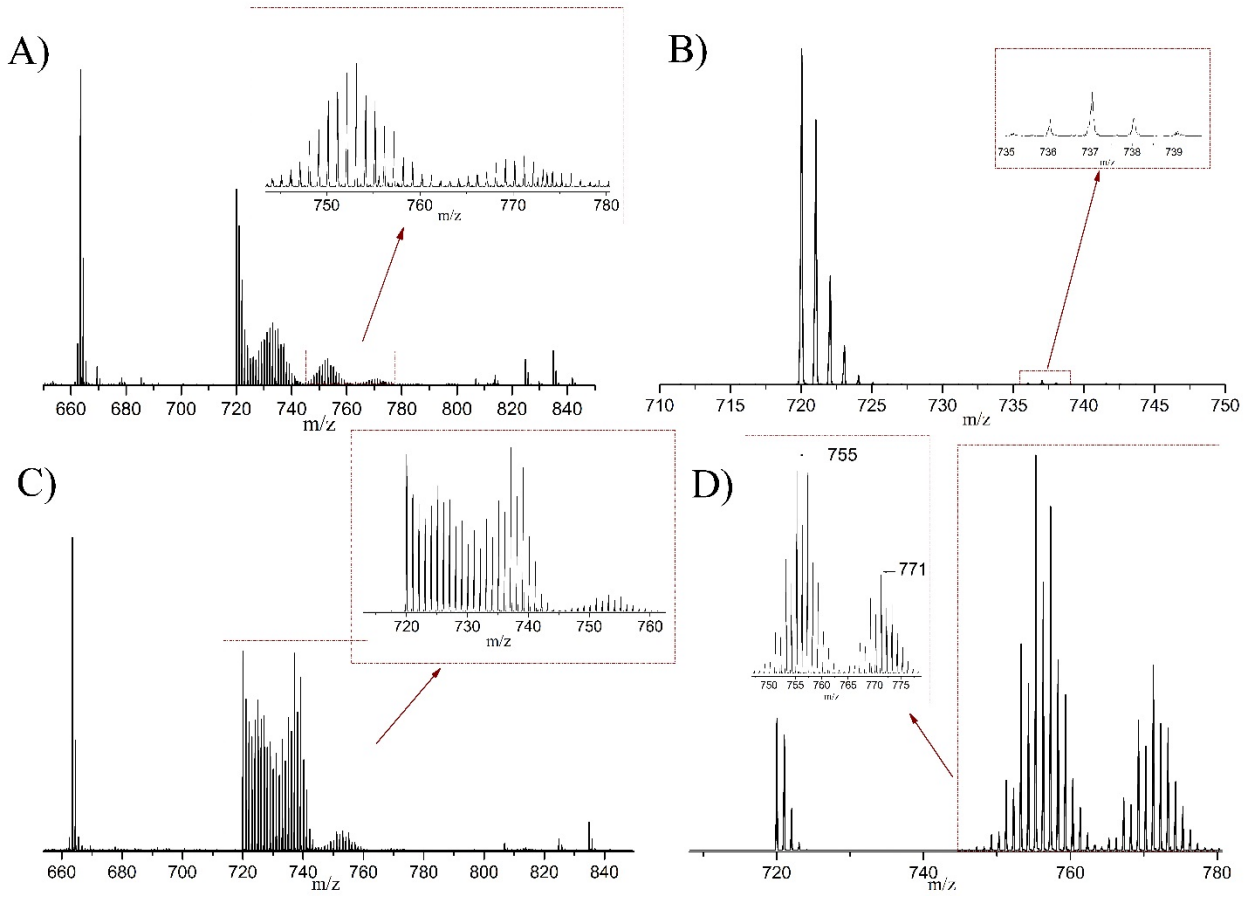

Figure 8: Positive mode APPI-MS spectra of A) $LiBH_4$:C_{60} as-prepared (heated solvent removal), B) $LiBH_4$:C_{60} dehydrogenated state, C) $LiBH_4$:C_{60} as prepared (no heat used in solvent removal), D) $C_{60}H_{36}$ (Birch Reduction)

It is also evident that C_{60} is present in the sample after 3 cycles, but by the 8th cycle the intensity of C_{60} ions is significantly reduced (Supporting Information). This suggests that the fullerene cage is further modified by cycling the material. This is possibly due to the formation of carbon-boron bonds and/or polymerization resulting in cage rupturing and irreversible fullerene alteration. The observed fulleranes are consistent with a degree of hydrogenation between $C_{60}H_{18}$ and $C_{60}H_{36,}$ which was also confirmed by LDI-TOF-MS. (Supporting Information) APPI-MS spectra of fulleranes with a toluene dopant have been shown to undergo a proton transfer to the fullerane resulting in mass peaks higher than that of the expected parent mass.[29] It was also found that the APPI-MS of $C_{60}H_{36}$, synthesized via the Birch reduction, also displayed higher than expected mass peaks. The higher mass distribution centered at ~751 m/z is likely due to the oxygenated species of $C_{60}H_x$.

3.6 FTIR

In figure 9, the FTIR spectrum shows that the B-H bending mode (~1100 cm^{-1}) and stretching modes (2200-2400 cm^{-1}) in both the as prepared and rehydrogenated $LiBH_4$-C_{60} samples. These peaks are absent in the dehydrogenated state and indicates the decomposition of the BH_4^- species. There is a slight broadening of the stretching modes in the as prepared and rehydrogenated samples which suggests an interaction between the BH_4^- and the C_{60} as suggested by theoretical calculations[16] as well as in other porous scaffolds.[15] The interaction

may also be indicated through the formation of new peak at ~2490 and ~1400 cm^{-1} in the as prepared and rehydrogenated samples. The multiple peaks below 1200 cm^{-1} in the as prepared and rehydrogenated sample could be attributed to multiple Li-B-H intermediate species that form during the initial reaction between $LiBH_4$ and C_{60} as well as during the subsequent dehydrogenation/rehydrogenation steps.[4, 30-32]

The infrared spectra also shows the presence of sp^3 hybridized C-H stretching modes in the region of 2850 cm^{-1} to 2950 cm^{-1} and C-H bending modes at ~1423 cm^{-1} for the "as prepared" and rehydrogenated materials. The disappearance of these peaks after dehydrogenation gives evidence that the fulleranes release the majority of their hydrogen after full desorption.

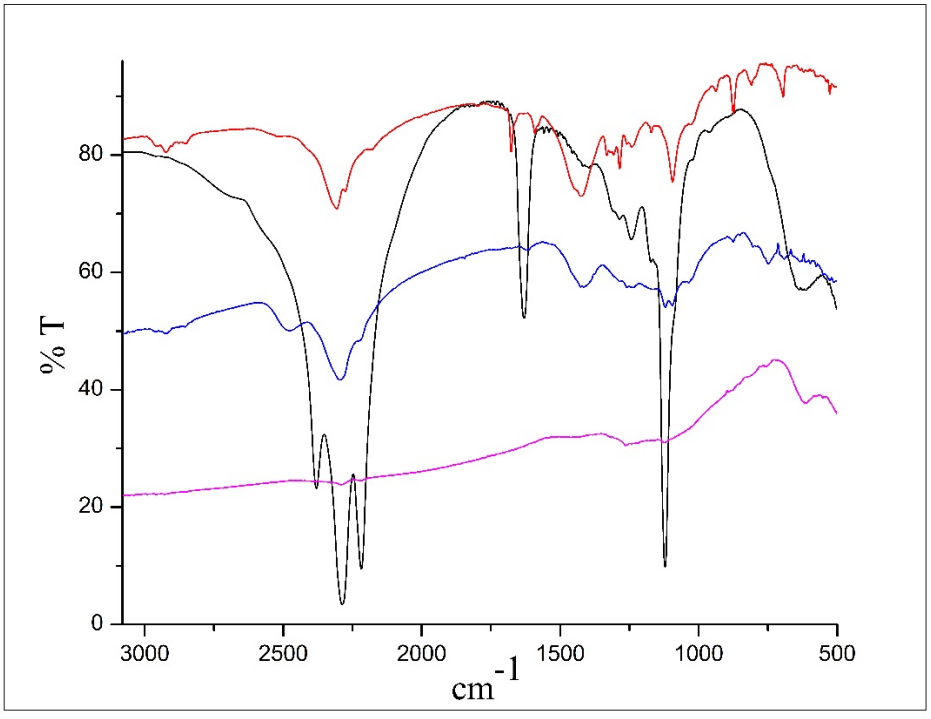

Figure 9. FT-IR spectra of pure $LiBH_4$ (black), $LiBH_4$:C_{60} as prepared (red), $LiBH_4$:C_{60} after the 2nd dehydrogenation (magenta), and $LiBH_4$:C_{60} after the 2nd hydrogenation (blue).

The rather low intensity and slightly differing peak positions of the C-H stretching modes, in comparison to other literature sources[33] is likely due to the relatively small amount of C_{60} in the composite (30%). The hydrogenated fullerenes are observed in APPI-MS and LDI-TOF-MS, but their low intensity in the IR spectra suggest that the ionization processes for the mass spectra may have been energetic enough to induce fullerane production. The F_{1u} vibrational modes of C_{60} (~527 cm^{-1}, 577 cm^{-1}, 1182 cm^{-1},1430 cm^{-1})[34] are not present in any considerable amount, suggesting significant cage modification in the preparation of the material.

3.7 ^{1}H NMR

Solution state ^{1}H NMR spectra, figure 10, shows the regeneration of $LiBH_4$ in the rehydrogenated material as evidenced by the reappearance of the BH_4 anion. In d_6-dimethylsulfoxide, the BH_4 protons have a chemical shifts between 0 and -0.6 ppm and the characteristic splitting pattern is due to spin-spin coupling with the ^{11}B (3/2) and ^{10}B (3) nuclei. The multiplicity (2S+1) of the ^{11}B coupled protons is 4 and 7 for the ^{10}B coupled protons, with the integrated areas under the peaks corresponding to their atomic abundance. It is also evident that $LiBH_4$ is completely consumed in the dehydrogenated material by the disappearance of the BH_4 proton signal. There is evidence of C-H protons in the as prepared and rehydrogenated material (supporting information), but the identification of these species is complicated by the fact that there is a likely a mixture fulleranes with different degrees of hydrogenation and multiple symmetries. For the purpose of this study, we simply use NMR to further illustrate the regeneration of $LiBH_4$.

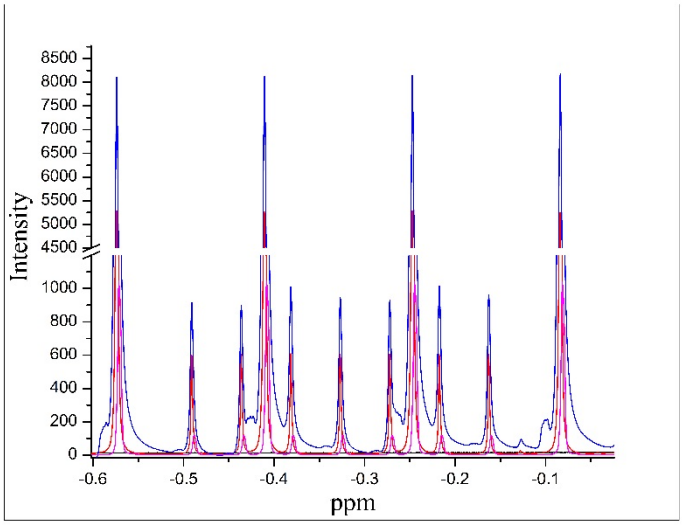

Figure 10: ^{1}H solution state NMR of the BH_4^{-1} region in d_6-Dimethylsufoxide for $LiBH_4$ (magenta), $LiBH_4$:C_{60} as prepared (red), $LiBH_4$:C_{60} rehydrogenated (blue), $LiBH_4$:C_{60} dehydrogenated (black).

3.8 XRD

XRD was also measured for the sample at various points during the hydrogen desorption/absorption cycles. Figure 11a shows that $LiBH_4$ is the primary component of the as prepared $LiBH_4$:C_{60} material. No diffraction peaks were detectible for C_{60} and indicates that its structure has been significantly modified through a combination of polymerization and hydrogenation. Dehydrogenation and rehydrogenation shows the disappearance and reappearance of $LiBH_4$ in the sample, respectively, with a noticeable decrease in peak intensity as cycling of the material is continued. On the other hand, there is a continued increase in the amount of LiH present in the material in both the rehydrogenated and dehydrogenated states with increasing number of cycles (Figure 11b). The accumulation of LiH in the material acts as dead weight contributing to the loss in hydrogen storage capacity and indicates an irreversible reaction

is occurring. There are two possible reasons why the amount of LiH is increasing in the samples with cycling. First, it is possible that during the dehydrogenation process volatile boron species (i.e. B_2H_6) are being generated which decreases the amount of available boron in the material for the reformation of $LiBH_4$. Although no volatile boron species were detected by our RGA interfaced with the TGA during desorption cycles, the current instrument set-up is not optimized for the detection of these species. Another possible explanation is that the temperatures and pressures utilized for rehydrogenation are not enough to promote the recombination of lithium hydride with boron and hydrogen ($LiH + B + 3/2\ H_2 \rightarrow LiBH_4$) due to the segregation of LiH and boron in the material after multiple cycles. These two decomposition mechanisms are consistent with the observed TGA-RGA data showing that the second desorption event becomes more dominant relative to the dehydrogenation of the regenerated $LiBH_4$ (first desorption event).

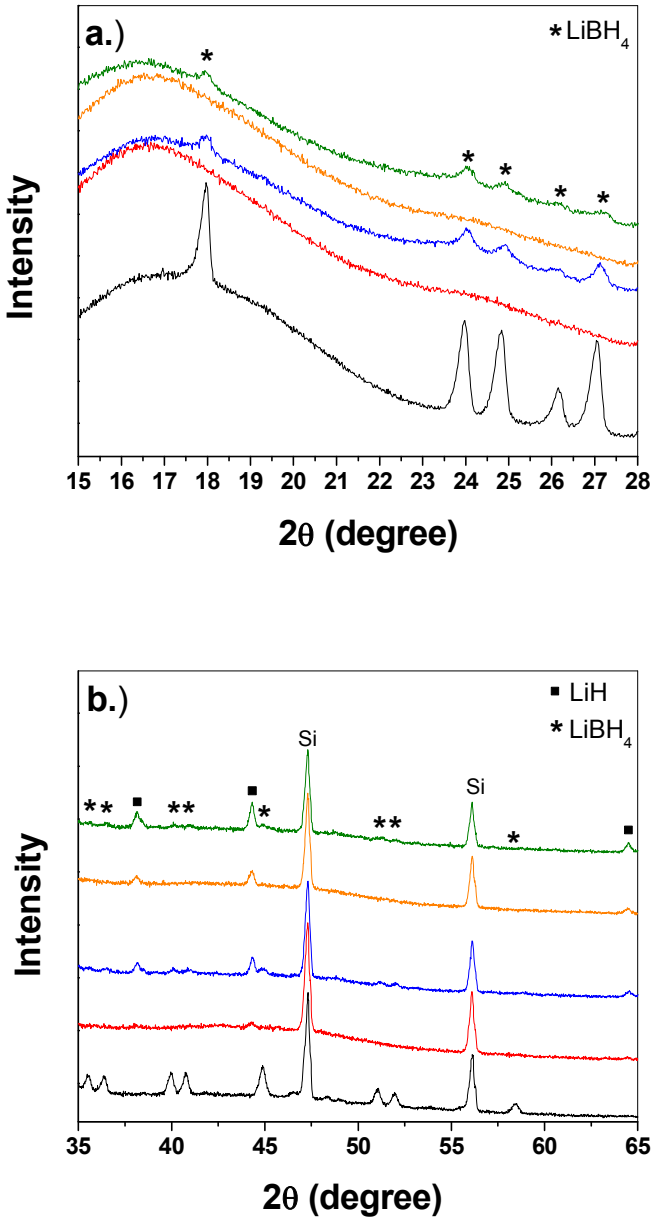

Figure 11: XRD spectra of the $LiBH_4$:C_{60} composite at various stages of cycling. Black- as prepared, Red- 1st dehydrogenation. Blue- 1st rehydrogenation, Orange- 2nd dehydrogenation, and green- 2nd rehydrogenation.

4. Conclusion

We have demonstrated that a $LiBH_4$:C_{60} nanocomposite prepared from a ball-mill free

solvent-assisted mixing method can reversibly store hydrogen over multiple cycles under relatively mild conditions. It was determined that C_{60} (reversibly forming C-H bonds) plays an active role in the hydrogen storage process in this material, unlike typical carbon based materials utilized for systems that rely solely on the nanoconfinment effect for regenerating $LiBH_4$. We propose that desorption of hydrogen from the material occurs in two steps, wherein, the hydrogen first desorbs from $LiBH_4$ in a lower energy mechanism on the fullerene surface followed by the dehydrogenation of the carbon species after the consumption of available $LiBH_4$. There is also direct evidence for a significant modification of the C_{60} structure even in the as prepared state in which there is polymerization as well as reduction of the fullerene to form a partially hydrogenated fullerene. The direct formation of C-H on C_{60} by $LiBH_4$ is not surprising due to the fact that it is known as an extremely powerful reducing agent in organic synthesis. A recent report has demonstrated that $LiAlH_4$, which is also a powerful reducing agent, is capable of directly forming C-H bonds during the reduction of graphene oxide.[35] The addition of C_{60} to $LiBH_4$ not only lowers the dehydrogenation temperature and enhances reversibility, but also provides another species in the material capable of reversibly storing hydrogen in C-H bonds.

Supporting Information. Additional LDI-TOF-MS and APPI-MS data in negative and positive mode is available. This material is available free of charge via the internet at http://pubs.acs.org.

Corresponding Author

*Ragaiy Zidan, Savannah River National Laboratory, Clean Energy Directorate, Aiken, SC 29803, Ph. +1 803-646-8876, email- ragaiy.zidan@srnl.doe.gov

ACKNOWLEDGMENT

J.A.T., R.Z., B.P., and J.W. would like to thank the DOE Office of Basic Energy Science. P.A.W. and R.N.C. would like to thank the National Science Foundation grant number DGE0801470, "Sustainable Technology through Advanced Interdisciplinary Research" (STAIR), awarded to the University of Tennessee Knoxville.

REFERENCES

1. Yan, Y.; Remhof, A.; Hwang, S. J.; Li, H. W.; Mauron, P.; Orimo, S.; Zuttel, A., *Phys. Chem. Chem. Phys.* **2012,** 14, 6514-6519.
2. Vajo, J. J.; Olsen, G. L., *Scr. Mater.* **2007,** 56, 829-834.
3. Li, C.; Peng, P.; Zhou, D. W.; Wan, L., *Int. J. Hydrogen Energy* **2011,** 36, 14512-14526.
4. Fang, Z.-Z.; Wang, P.; Rufford, T. E.; Kang, X. D.; Lu, G. Q.; Cheng, H. M., *Acta Mater.* **2008,** 56, 6257-6263.
5. Zhang, Y.; Zhang, W. S.; Wang, A. Q.; Sun, L. X.; Fan, M. Q.; Chu, H. L.; Sun, J. C.; Zhang, T., *Int. J. Hydrogen Energy* **2007,** 32, 3976-3980.
6. Yu, X. B.; Wu, Z.; Chen, Q. R.; Li, Z. L.; Weng, B. C.; Huang, T. S., *Appl. Phys. Lett.* **2007,** 90, 034106.
7. Fang, Z.-Z.; Kang, X. D.; Wang, P.; Cheng, H. M., *J. Phys. Chem. C* **2008,** 112, 17023-17029.
8. Wang, P.-J.; Fang, Z.-Z.; Ma, L.-P.; Kang, X.-D.; Wang, P., *Int. J. Hydrogen Energy* **2008,** 33, 5611-5616.
9. Gross, A. F.; Vajo, J. J.; Van Atta, S. L.; Olsen, G. L., *J. Phys. Chem. C* **2008,** 112, 5651-5657.
10. Ngene, P.; Adelhelm, P.; Beale, A. M.; de Jong, K. P.; de Jong, P. E., *J. Phys. Chem. C* **2010,** 114, 6136-6138.
11. Liu, X.; Peaslee, D.; Jost, C. Z.; Majzoub, E. H., *J. Phys. Chem. C* **2010,** 114, 14036-14041.
12. Wang, P. J.; Fang, Z. Z.; Ma, L. P.; Kang, X. D.; Wang, P., *Int. J. Hydrogen Energy* **2010,** 35, 3072-3075.
13. Nielsen, T. K.; Bosenberg, U.; Dornheim, M.; Cerenius, Y.; Besenbacher, F.; Jensen, T. R., *ACS Nano* **2010,** 4, 3903-3908.
14. Liu, X.; Peaslee, D.; Jost, C. Z.; Baumann, T. F.; Majzoub, E. H., *Chem. Mater.* **2011,** 23, 1331-1336.
15. Sun, T.; Liu, J.; Jia, Y.; Wang, H.; Sun, D.; Zhu, M.; Yao, X., *Int. J. Hydrogen Energy* **2012,** 37, 18920-18926.
16. Scheicher, R. H.; Li, S.; Araujo, C. M.; Blomqvist, A.; Ahuja, R.; Jena, P., *Nanotechnology* **2011,** 22, 335401.
17. Teprovich Jr., J. A.; Wellons, M.; Lascola, R.; Hwang, S.; Ward, P.; Compton, R.; Zidan, R., *Nano Lett* **2012,** 12, 582-589.

18. Teprovich Jr., J. A.; Knight, D. A.; Wellons, M. S.; Zidan, R., *J. Alloys Compd.* **2011,** 509S, S562-S566.
19. Wellons, M. S.; Berseth, P. A.; Zidan, R., *Nanotechnology* **2009,** 20, 204022.
20. Berseth, P. A.; Harter, A. G.; Zidan, R.; Blomqvist, A.; Araujo, C. M.; Scheicher, R. H.; Ahuja, R.; Jena, P., Carbon Nanomaterials as. *Nano Letters* **2009,** 9, (4), 1501-1505.
21. Shane, D. T.; Corey, R. L.; Bowman, R. C.; Zidan, R.; Stowe, A. C.; Hwang, S.; Kim, C.; Conradi, M. S., *J. Phys. Chem. C* **2009,** 113, 18414-18419.
22. Paolone, A.; Vico, F.; Teocoli, F.; Sanna, S.; Palumbo, O.; Cantelli, R.; Knight, D. A.; Teprovich Jr., J. A.; Zidan, R., *J. Phys. Chem. C* **2012,** 116, 16365-16370.
23. Teprovich Jr, J. A.; Knight, D. A.; Peters, B.; Zidan, R., J. Alloys Comp. (2013), http://dx.doi.org/10.1016/j.jallcom.2013.02.024.
24. Paolone, A.; Palumbo, O.; Leardini, F.; Cantelli, R.; Knight, D. A.; Teprovich, J., J.A.; Zidan, R., J. Alloys Comp. (2013), doi: http://dx.doi.org/10.1016/j.jallcom.2013.03.162. **2013**.
25. Knight, D. A.; Teprovich Jr., J. A.; Summers, A.; Peters, B.; Ward, P. A.; Compton, R. N.; Zidan, R., 2013, Nanotechnology (in Press).
26. Kissinger, H. E., *Anal. Chem.* **1957,** 29, 1702-1706.
27. Zuttel, A.; Rentsch, S.; Fischer, P.; Wenger, P.; Sudan, P.; Mauron, P.; Emmenegger, C., *Journal of Alloys and Compounds* **2003,** 356-357, 515-520.
28. Orimo, S.; Nakamori, Y.; Kitahara, G.; Miwa, K.; Ohba, N.; Towata, S.; Zuttel, A., Dehydriding and rehydriding reactions of LiBH4. *J. Alloys Compd.* **2005,** 404-406, 427-430.
29. Nunez, O.; Gallart-Ayala, H.; Martins, C. P. B.; Moyano, F.; Galceran, M. T., *Anal. Chem.* **2012,** 84, 5316-5326.
30. Orimo, S.; Nakamori, Y.; Ohba, N.; Miwa, K.; Aoki, M.; Towata, S.; Zuttel, A., *Appl. Phys. Lett.* **2006,** 89, 021920.
31. Ohba, N.; Miwa, K.; Aoki, M.; Noritake, T.; Towata, S.; Nakamori, Y.; Orimo, S.; Zuttel, A., *Phys. Rev. B* **2006,** 74, 075110.
32. Pitt, M. P.; Paskevicius, M.; Brown, D. H.; Sheppard, D. A.; Buckley, C. E., *J. Am. Chem. Soc.* **2013,** 135, 6930-6941.
33. Bini, R.; Ebenhoch, J.; Fanti, M.; Fowler, P. W.; Leach, S.; Orlandi, G.; Ruchardt, C.; Sandall, J. P. B.; Zerbetto, F., *Chem. Phys.* **1998,** 232, 75-94.
34. Ajie, H.; Alvarez, M. M.; Anz, S. J.; Beck, R. D.; Diederich, F.; Fostiropoulos, K.; Huffman, D. R.; Kratschmer, W.; Rubin, Y.; Schriver, K. E.; Sensharma, D.; Whetten, R. L., *J. Phys. Chem.* **1990,** 94, 86308633.
35. Ambrosi, A.; Chua, C. K.; Bonanni, A.; Pumera, M., *Chem. Mater.* **2012,** 24, 2292-2298.

SYNOPSIS (Word Style "SN_Synopsis_TOC"). If you are submitting your paper to a journal that requires a synopsis, see the journal's Instructions for Authors for details.